Progress In Electromagnetics Research, Vol. 154, 87–100, 2015

Performance of the Reflectivity Measurement in a Reverberation Chamber

Angelo Gifuni[1, *], Horiya Khenouchi[2], and Gilda Schirinzi[1]

Abstract—The reflectivity measurement of materials is an innovative application of a reverberation chamber (RC). In this paper we show an analysis of the performance of the reflectivity measurement in an RC in terms of uncertainty of measurement and relevant noise level. The model for reflectivity measurement, which is already present in literature, is based on the absorption cross section (ACS) measurements. If the ACS measurements are averaged with respect to the configurations of the measurement system, then the relevant uncertainty depends only on the number of independent samples. Here, the performance of the reflectivity measurements is shown in cases where it depends only on the number of independent samples acquired in an RC. Simulations and measurements confirm the validity of the expected results.

1. INTRODUCTION

A reverberation chamber (RC) is an attractive testing facility [1], which simulates realistic test environments [2]. Various applications have already been available [1], and others are being studied. In particular, applications for radiate power measurements are shown in [3]; applications for shielding effectiveness measurements are shown in [4–13]; applications for absorption measurements are shown in [14–19]; applications for radiation efficiency measurements of antennas are shown in [20–22]; studies for the testing of wireless devices by emulations of a Rician radio environment are shown in [23–26]. The reflectivity measurement of materials is certainly an innovative application of an RC. The absorbing surface method for the reflectivity measurements in an RC was developed in [15], and some initial results on the metallic mesh grid and fabric and nonwoven fabric are shown in [27, 28]. This method uses a high-quality microwave absorber to create an equivalent free space between a plane sample of the material under test and the surface of the absorber, so that the reflected energy by the sample is separated from the one transmitted through it; the ratio between the former and the incident one, which represents the reflectivity coefficient of the sample under test, can be estimated by a simple measurement procedure [15]. However, no analysis of the performance of the measurement method in terms of measurement uncertainty and relevant noise level (NL) has been systematically done so far. The procedure considers three absorption cross section (ACS) measurements, which are achieved by as many measurements of insertion loss (IL). Note that in this paper the IL is defined so that its value in dB turns out to be negative. The uncertainty of an ACS measurement depends on the configuration of the measurement system as well [22]; the component of uncertainty due to the configuration is connected to any non-uniformity of the field, both without and with the sample present in the chamber. However, in light of the fact that the ACS measurements can be made so that the relevant uncertainty depends only on the number of independent samples (N) that can be acquired in an RC [22], the performance

Received 29 July 2015, Accepted 26 October 2015, Scheduled 10 December 2015

* Corresponding author: Angelo Gifuni (angelo.gifuni@uniparthenope.it).

[1] Dipartimento di Ingegneria, Università degli Studi di Napoli "Parthenope", Napoli 80143, Italy. [2] Laboratory of Image Processing and Radiation (LTIR), Electronics and Computer Science Faculty, University of Sciences and Technology Houari Boumediene (USTHB), Bab Ezzouar-Algiers, Algeria.

of the reflectivity measurement is shown here in terms of measurement uncertainty and relevant NL in cases where it is due only to N. It is important to note that the samples (N) can be increased and acquired as mentioned above, by using a combination of stirring techniques [14, 22].

The reflectivity measurements can also be made in an anechoic chamber (AC). But, we stress that for some applications, as those in the field of the electromagnetic compatibility (EMC), it is important to know the average value of the parameter to be measured with respect to the direction and polarization of the incident field, as shown in [3]. In such cases, the use of RCs, which are also cheaper than the ACs, is advantageous.

2. ESTIMATE OF THE MEASUREMENT UNCERTAINTY

In this section, the estimate of the uncertainty of the reflectivity measurement in an RC is shown. We specify that the estimate is made by considering that the independent samples are acquired so that the uncertainty due to the system configuration of measurement is properly neutralized [22]. In this case, the estimate depends only on N [22].

The reflectivity (R) is achieved by the combination of three measurements of IL [15], then three ACS measurements are obtained: the ACS of the empty chamber and the ACSs of the absorbing surface with sample and with no sample under test [21, 22]. We specify that normally a measurement of ACS requires the corrections for radiation and total efficiency, whereas the measurement of reflectivity does not require such corrections, as it is achieved by uniform ratios [22].

The mathematical model of the measurement method, which is shown here using simplified symbols with respect to those used in [15], can be written as follows [15, 22]:

$$R = \frac{A_a - A_{a,S}}{A_a} = \frac{IL_e}{IL_{a,S}} \frac{IL_{a,S} - IL_a}{IL_e - IL_a}, \tag{1}$$

where $A_a = A_a^{eq,A}$ in [15] is the ACS of the absorbing surface; $A_{a,S} = A_a^{eq,AS_1}$ in [15] is the ACS of the absorbing surface with the sample under test. $IL_e = IL^{rc0}$ in [15] is the IL when the absorbing surface is not present in the RC; $IL_a = IL^{eq,A}$ and $IL_{a,S} = IL^{eq,AS_1}$ in [15] are the ILs when the surface without sample and with sample is present in the RC, respectively. Only samples with symmetric ACS are considered here. However, for samples with asymmetric ACS, it is sufficient to repeat the measurement procedure for both the sides of the sample under test to achieve both the reflectivity coefficients [15].

The ILs, IL_e, IL_a, and $IL_{a,S}$ are sample means with respect to the relevant populations, which are chi-squared distributed with two degrees of freedom; they are obtained by a number of independent samples N acquired to a given frequency. Therefore, such ILs are independent random variables (RVs), and their probability density function (PDF) is Gaussian, whose means and variances are known, as the PDFs of the populations are well-known. In short, by denoting with $IL_{e,0}$, $IL_{a,0}$, and $IL_{a,S,0}$ the mean values of the relative populations, the means and variances of the Gaussian distributions are just $IL_{e,0}$, $IL_{a,0}$, $IL_{a,S,0}$ and $(IL_{e,0})^2/N$, $(IL_{a,0})^2/N$, $(IL_{a,S,0})^2/N$, respectively. We specify that we consider $IL_{e,0}$ ≤ 0.1 ($IL_{e,0} \leq -10\,\mathrm{dB}$) as an acceptable condition of uniformity and isotropy of the field; similarly, for its PDF.

Equation (1) can be written as follows:

$$R = \frac{IL_e}{IL_{a,S}} \frac{IL_{a,S} - IL_a}{IL_e - IL_a} = \frac{IL_e IL_{a,S} - IL_e IL_a}{IL_{a,S} IL_e - IL_{a,S} IL_a} = \frac{L}{M}, \tag{2}$$

where $L = IL_e IL_{a,S} - IL_e IL_a$ and $M = IL_{a,S} IL_e - IL_{a,S} IL_a$. By setting $X = IL_e IL_{a,S}$, $Y = IL_e IL_a$, $V = IL_{a,S} IL_e$, and $Z = IL_{a,S} IL_a$, we find that the RVs X and Y are correlated, as well as V and Z; the PDFs of X, Y, V, and Z are approximately Gaussian [29] and the relevant means and variances are also known [29]. The RVs L and M are correlated; the correlation coefficient depends on the values $IL_{e,0}$, $IL_{a,0}$, and $IL_{a,S,0}$. The mean and variance of R can be written in analytical form [29, 30]. In the next section, the analytical (expected) results are compared with the numerical simulation results. Both the analytical and numerical simulations shown in this paper are achieved by using LabVIEW from National Instruments (NI). Actually, all the assertions made here were verified by simulations as well.

The mean and standard deviation of R are calculated in the development below by statistical considerations. We specify that μ, σ, C, and ρ denote the mean, standard deviation, covariance, and correlation coefficient of the attendant RVs, respectively. Clearly, σ^2 denotes the variance of the attendant RV.

We can write [30]:

$$\begin{aligned} C(L,M) &= \mu_{LM} - \mu_L \mu_M \\ &= 2\frac{(IL_{e,0})^2 (IL_{a,S,0})^2}{N} - \frac{IL_{e,0} IL_{a,0} (IL_{a,S,0})^2}{N} - \frac{(IL_{e,0})^2 IL_{a,0} IL_{a,S,0}}{N} + \frac{(IL_{a,0})^2 IL_{e,0} IL_{a,S,0}}{N}, \end{aligned} \quad (3)$$

$$\rho(L,M) = \frac{C(L,M)}{\sigma_L \sigma_M} = \frac{2 - \dfrac{IL_{a,0}}{IL_{a,S,0}} + \dfrac{(IL_{a,0})^2}{IL_{e,0} IL_{a,S,0}} - \dfrac{IL_{a,0}}{IL_{e,0}}}{2\sqrt{1 + \left(\dfrac{IL_{a,0}}{IL_{a,S,0}}\right)^2 - \dfrac{IL_{a,0}}{IL_{a,S,0}}} \sqrt{1 + \left(\dfrac{IL_{a,0}}{IL_{e,0}}\right)^2 - \dfrac{IL_{a,0}}{IL_{e,0}}}}, \quad (4)$$

$$\mu_{L/M} = \mu_{R_r} = \frac{\mu_L}{\mu_M} + \frac{\sigma_M^2 \mu_L}{(\mu_M)^3} - \rho(L,M)\frac{\sigma_L \sigma_M}{(\mu_M)^2} = \frac{\mu_L}{\mu_M} + \frac{\sigma_M^2 \mu_L}{(\mu_M)^3} - C(L,M)\frac{1}{(\mu_M)^2}, \quad (5)$$

$$\sigma_{L/M}^2 = \sigma_{R_r}^2 = \frac{\sigma_L^2}{(\mu_M)^2} + \frac{\sigma_M^2 (\mu_L)^2}{(\mu_M)^4} - 2\rho(L,M)\frac{\sigma_L \sigma_M \mu_L}{(\mu_M)^3} = \frac{\sigma_L^2}{(\mu_M)^2} + \frac{\sigma_M^2 (\mu_L)^2}{(\mu_M)^4} - 2C(L,M)\frac{\mu_L}{(\mu_M)^3}, \quad (6)$$

where

$$\begin{aligned} \mu_L &= IL_{e,0} IL_{a,S,0} - IL_{e,0} IL_{a,0}, \\ \mu_M &= IL_{a,S,0} IL_{e,0} - IL_{a,S,0} IL_{a,0}, \\ \sigma_L &= \left\{ \frac{2}{N} (IL_{e,0})^2 \left[(IL_{a,S,0})^2 + (IL_{a,0})^2 - IL_{a,S,0} IL_{a,0} \right] \right\}^{1/2}, \\ \sigma_M &= \left\{ \frac{2}{N} (IL_{a,S,0})^2 \left[(IL_{e,0})^2 + (IL_{a,0})^2 - IL_{e,0} IL_{a,0} \right] \right\}^{1/2}. \end{aligned}$$

We can write [30]:

$$\mu_R = R_0 \left(1 + \frac{\sigma_M^2}{(\mu_M)^2} \right) - C(L,M)\frac{1}{(\mu_M)^2}, \quad (7)$$

$$\sigma_R^2 = \frac{\sigma_L^2}{(\mu_M)^2} \left[1 + R_0^2 \frac{\sigma_M^2}{\sigma_L^2} - 2R_0 \frac{C(L,M)}{\sigma_L^2} \right], \quad (8)$$

where

$$R_0 = \frac{\mu_L}{\mu_M} = \frac{IL_{e,0} IL_{a,S,0} - IL_{e,0} IL_{a,0}}{IL_{a,S,0} IL_{e,0} - IL_{a,S,0} IL_{a,0}}. \quad (9)$$

Finally, we can write:

$$\mu_R = R_0 \left[1 + \frac{2}{N} \frac{\left[1 + \dfrac{(IL_{a,0})^2}{(IL_{e,0})^2} - \dfrac{IL_{a,0}}{IL_{e,0}} \right]}{\left(1 - \dfrac{IL_{a,0}}{IL_{e,0}} \right)^2} \right] - \frac{1}{N} \left\{ \frac{\left[2 - \dfrac{IL_{a,0}}{IL_{e,0}} \right]}{\left(1 - \dfrac{IL_{a,0}}{IL_{e,0}} \right)^2} + \frac{\dfrac{IL_{a,0}}{IL_{a,S,0}} \left[\dfrac{IL_{a,0}}{IL_{e,0}} - 1 \right]}{\left(1 - \dfrac{IL_{a,0}}{IL_{e,0}} \right)^2} \right\}, \quad (10)$$

$$\sigma_R^2 = \frac{2}{N} \frac{\left[1 + \dfrac{(IL_{a,0})^2}{(IL_{a,S,0})^2} - \dfrac{IL_{a,0}}{IL_{a,S,0}} \right]}{\left(1 - \dfrac{IL_{a,0}}{IL_{e,0}} \right)^2} \left\{ 1 + R_0^2 \frac{\left[1 + \dfrac{(IL_{a,0})^2}{(IL_{e,0})^2} - \dfrac{IL_{a,0}}{IL_{e,0}} \right]}{\left[1 + \dfrac{(IL_{a,0})^2}{(IL_{a,S,0})^2} - \dfrac{IL_{a,0}}{IL_{a,S,0}} \right]} \right.$$

$$+R_0\frac{\left[\frac{IL_{a,0}}{IL_{a,S,0}}-2\right]}{\left[\left(\frac{IL_{a,0}}{IL_{a,S,0}}\right)^2-\frac{IL_{a,0}}{IL_{a,S,0}}+1\right]}+R_0\frac{\frac{IL_{a,S,0}}{IL_{e,0}}\left[\frac{IL_{a,S,0}}{IL_{a,0}}-1\right]}{\left[\left(\frac{IL_{a,S,0}}{IL_{a,0}}\right)^2-\frac{IL_{a,S,0}}{IL_{a,0}}+1\right]}\Bigg\}. \tag{11}$$

Note that for $N \gg 1$, we can write (see Fig. 3(b) in the next section):

$$\mu_R \cong R_0. \tag{12}$$

Note also that σ_R^2 tends to $2/N$ when $IL_{a,S,0}$ tends to $IL_{a,0}$; that is, σ_R^2 tends to $2/N$ for small values of R; $\sqrt{2/N}$ is the worst standard uncertainty for R when N is fixed [31]. The optimal range of values of the ratio $IL_{e,0}/IL_{a,0}$ is shown and discussed below. Note that the systematic error due to the average residual reflectivity of a real absorber [15] is not discussed here. However, when it is necessary, such a systematic error can be properly removed.

3. ANALYTICAL AND NUMERICAL SIMULATION RESULTS

By mathematical model (1), in terms of both ACSs and *IL*s, we note that the difference in the numerator affects the measurement dynamic range. The latter can be improved by increasing $A_{a,0}$ (or equivalently by reducing $IL_{a,0}$), which is the sample mean of A_a, compatibly with the necessary conditions of uniformity and isotropy of the field, and/or the independent sample number to be acquired for each frequency point. Unfortunately, the increase of dynamic range is not very sensible with respect to both the expedients. In particular, the sensibility of the improvement decreases with the increase of $A_{a,0}$, as can be seen by the connection between *IL* and ACS (see Fig. 1 below as well), whereas it increases with the reciprocal of the root of N (see Fig. 1). Therefore, when the max load (the acceptable max value for $A_{a,0}$ or the acceptable minimum value for $IL_{a,0}$) of an RC is reached, only the independent sample number can be increased. The former implies the use of a large absorber, whereas the latter implies the acquisition of a very high number of independent samples. By considering the values in dB, one can replace the ratios in Eqs. (10)–(11) with differences. Here, the *IL*s are considered both in dB and in absolute value according to the context. In order to realize the appropriate range of differences in dB between $IL_{a,S,0}$ and $IL_{a,0}$, we first show the NL achieved by numerical simulations for given values of N and T, where this last one denotes the number of trials (sample means). Then, we represent the mean and standard uncertainty of R, which are given by Eq. (10) and the square root of Eq. (11), respectively [31], and compare them with the numerically simulated ones.

The NL is achieved when the sample under test is not present on the absorbing surface or when it is totally transparent; therefore, in such conditions, when N is fixed and T measurements are made (each with N samples acquired), we can assume that NL is equal to the max value of R. We specify that the NL of R has been here achieved by taking the absolute value of the numerator in Eq. (1) (or Eq. (2)), so as to express it in dB in any case. We stress that the absolute value of the numerator in Eq. (1) is taken for the NL calculation only. Such a procedure determines probabilistically a worse NL with the same N. In other words, such a definition includes all the values of NL. The measurement dynamic in dB could be taken equal to the opposite of the NL in dB (the max value of R is 0 dB). Strictly, the NL does not represent the dynamic range of the R measurement. The former determines the measurement range, which is the range of values that can be measured under any circumstances, whereas the latter is the range of values that can be measured to a specified uncertainty. However, the measurement dynamic range is often assumed to be equal to the NL, when this last one is defined as mentioned above.

Note that in the simulations T represents the number of sample means and N the sample size.

Figure 1 shows the maximum values of the NLs achieved by numerical simulations. They are achieved by using 10^4 sample means ($T = 10^4$), which are in turn achieved by 10^4, 10^5, and 10^6 independent samples (N). We specify that the numerical simulations are easily implemented as the statistics of the above-mentioned *IL*s are known. Therefore, for each *IL*, which is a sample mean with sample size N, T appropriate statistical samples are generated; the next statistical implementations and the relevant calculations are obvious and made by the software. It can be noted that the NL does

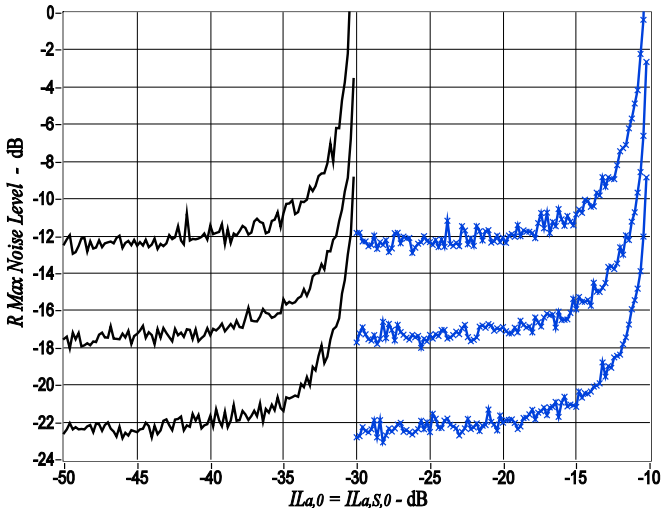

Figure 1. NL by numerical simulation. Max NLs of R as a function of $IL_{a,0}$ and for different values of N. For left traces, $IL_{e,0} = -30\,\text{dB}$; from up to down, N is 10^4, 10^5, and 10^6. For right traces, $IL_{e,0} = -10\,\text{dB}$; from up to down, N is 10^4, 10^5, and 10^6 again. The y-scale is limited to zero dB. $T = 10^4$ for all the traces. For each point, the NL represents the max value of R achieved by the T values of sample means.

not depend on $IL_{e,0}$, when N is fixed, but it depends on the difference in dB between $IL_{e,0}$ and $IL_{a,0}$, which determines $A_{a,0}$. In particular, it can be noted that the speed of the decrease of NL decreases with the increasing of the ratio $IL_{e,0}/IL_{a,0}$, as mentioned above, so that for $IL_{e,0}/IL_{a,0} \geq 10\,\text{dB}$, the NL can be considered practically constant with the same N. By Eq. (1), we see that if $IL_e \gg IL_a$, then it can be written:

$$R = \frac{IL_e}{IL_e - IL_a}\left(1 - \frac{IL_a}{IL_{a,S}}\right) \cong 1 - \frac{IL_a}{IL_{a,S}}. \tag{13}$$

By considering the conservation of the uniformity and isotropy of the field, Fig. 1 shows that the ratio $IL_{e,0}/IL_{a,0}$ of $6 \div 8\,\text{dB}$ is a good compromise. Such differences are certainly practicable in an RC [32]. However, if it is possible, it is better to use larger differences. Henceforward, we consider a ratio $IL_{e,0}/IL_{a,0}$ of 6 dB, as it is about equal to the ratio achieved in the experiments made for this paper, in the frequency range 1–10 GHz, by using an available absorber, as shown below (see Figs. 7 and 8).

Figures 2(a), 2(b), and 2(c) show typical details of the NL for N equal to 10^4, 10^5, and 10^6, respectively; T ranges from 1 to 10^4 for all the three figures. $IL_{a,0}$ was assumed equal to $-30\,\text{dB}$, and a difference of 6 dB between $IL_{e,0}$ and $IL_{a,0}$ is considered. Note that the NL of R has been achieved by taking the absolute value of the numerator in Eq. (1) (or Eq. (2)) again, so as to express it in dB in any case, as mentioned above.

Figure 3(a) shows the comparison between the analytical and numerical simulations of μ_R for $N = 10000$. For the numerically simulated trace $T = 10000$. The analytical simulation gives the expected results. We note that the two traces are all overlapped.

Figure 3(b) shows the comparison between μ_R and R_0 as a function of R_0 for $N = 1000$. We specify that for $N \geq 5000$, the traces of μ_R and R_0 are all overlapped, as mentioned above and as shown in Fig. 3(a) (see Eq. (12)).

Figure 4 shows the numerical and analytical simulations of the standard uncertainty of R under the same conditions of Figs. 2(a), 2(b), and 2(c). The standard uncertainty is expressed as a function of μ_R, where the last one is obtained by 10000 sample means ($T = 10000$), so, μ_R is de facto equal to R_0. We can note a good agreement between the results of the analytical and numerical simulations.

By Fig. 4, we find that the more R_0 is close to 0 dB, the more the standard uncertainty decreases, and it can be considered practically constant for about $R_0 < -8\,\text{dB}$.

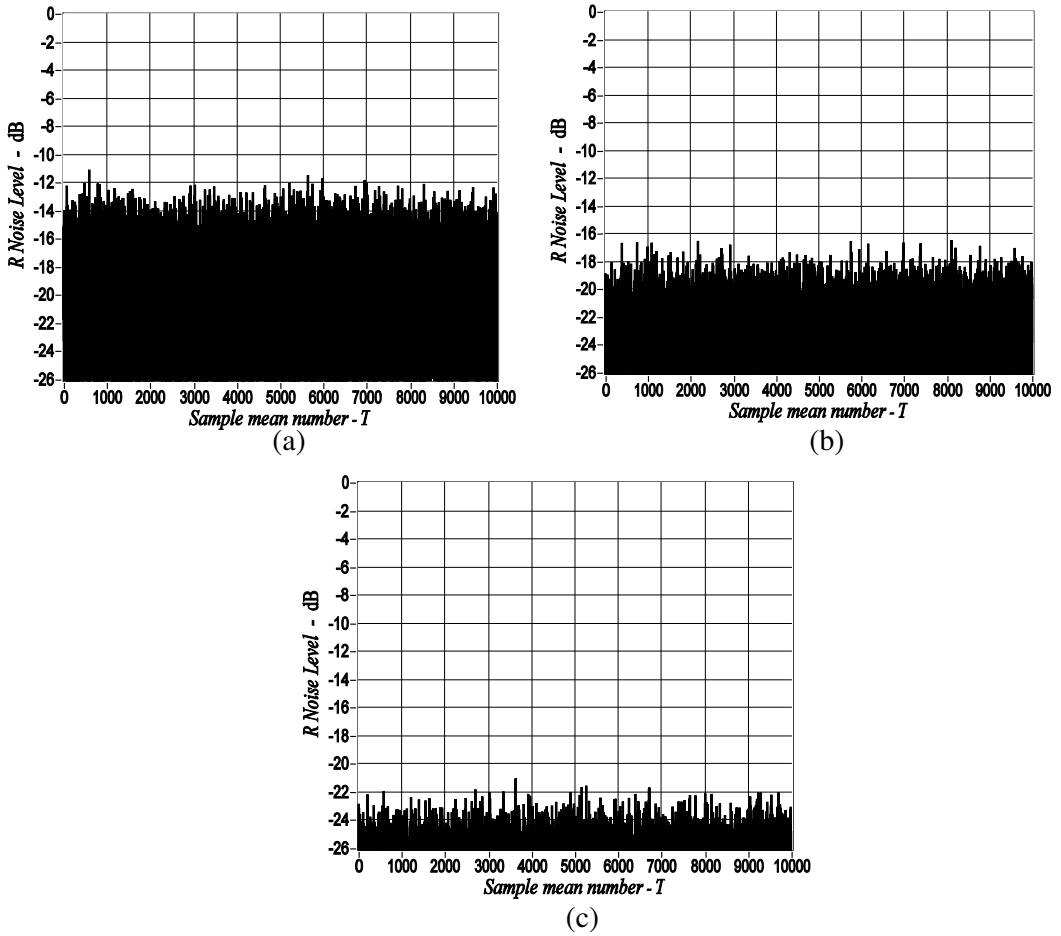

Figure 2. (a) NL by numerical simulation. The sample mean number (T) ranges from 1 to 10^4, and each sample mean is achieved by as many independent samples ($N = T = 10^4$). A difference of 6 dB between $IL_{e,0}$ and $IL_{a,0}$ is considered. (b) NL by numerical simulation. The sample mean number (T) ranges from 1 to 10^4, and each sample mean is achieved by 10^5 independent samples ($N = 10^5$). A difference of 6 dB between $IL_{e,0}$ and $IL_{a,0}$ is considered. (c) NL by numerical simulation. The sample mean number (T) ranges from 1 to 10^4, and each sample mean is achieved by 10^6 independent samples ($N = 10^6$). A difference of 6 dB between $IL_{e,0}$ and $IL_{a,0}$ is considered.

Figure 5 shows the numerical and analytical simulations of the variation coefficient of R as a function of R_0 again; it represents the relative standard uncertainty [31]. $IL_{e,0}$ and $IL_{a,0}$ are constant and equal to -30 dB and -36 dB, respectively; $IL_{a,S,0}$ ranges from -35.98 dB to -30 dB, so that R_0 changes consequentially.

We specify that the graphs in Figs. 4 and 5 can also be read as expanded uncertainty and expanded relative uncertainty, respectively, by adding $10 \log k$, where k is the coverage factor [31]. For example, if a confidence level of 99.73 percent is desired, then $k = 3$ and one must add $10 \log 3 = 4.77$ dB to the above-mentioned trace. Note that a normal distribution is considered for R, as shown in the appendix.

By considering the conditions of the traces in Fig. 5, one can set a max relative standard uncertainty (worst case) and find the corresponding measurement dynamic range. For example, by setting a relative standard uncertainty equal to -6 dB, which corresponds to 0.25, one achieves a measurement dynamic range about 11.5 dB, 16 dB and 21 dB, respectively. Similarly, by choosing a relative standard uncertainty of -10 dB, the measurement dynamic range turns out to be about 8, 12 and 17 dB, respectively. Clearly, these results can be achieved for any value of N and of the ratio $IL_{e,0}/IL_{a,0}$.

In principle, the results corresponding to the numerical simulations can be achieved by real

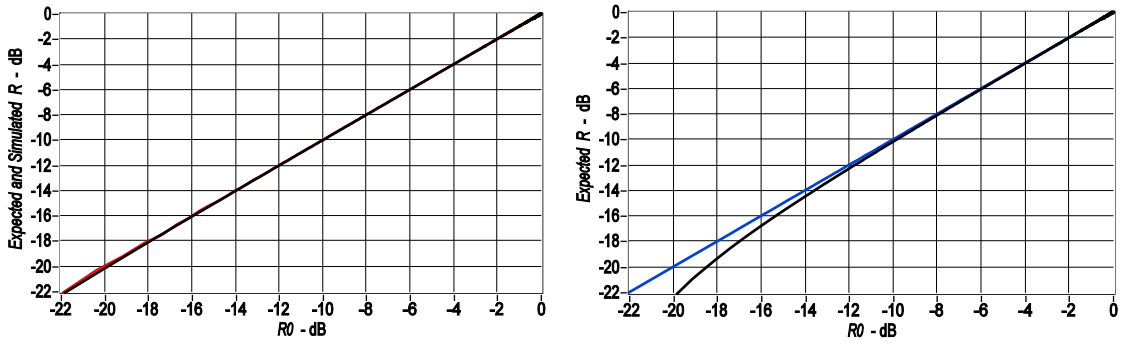

(a) (b)

Figure 3. (a) Analytical and numerical simulations of μ_R. The black trace is analytically simulated, whereas the red trace is numerically simulated. $IL_{e,0} = -30\,\text{dB}$; $IL_{e,0} - IL_{a,0} = 6\,\text{dB}$; $IL_{a,S,0}$ ranges from -30 to $-35.98\,\text{dB}$, so that R changes consequentially. $N = 10^4$. For the trace numerically simulated, $T = 10000$. (b) Analytical simulations of μ_R (lower trace) and R_0 (upper trace). $IL_{e,0} = -30\,\text{dB}$; $IL_{e,0} - IL_{a,0} = 6\,\text{dB}$; $IL_{a,S,0}$ ranges from -30 to $-35.98\,\text{dB}$, so that R changes consequentially. $N = 10^3$. For $N \geq 5000$, the traces of μ_R and R_0 are all overlapped.

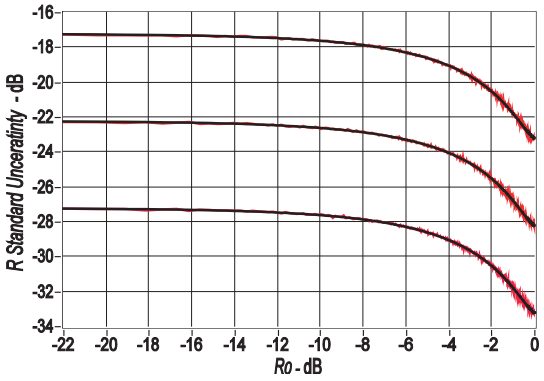

Figure 4. Numerical and analytical simulations of the standard uncertainty of R. The black traces are analytically simulated, whereas the red traces are numerically simulated. $IL_{e,0} = -30\,\text{dB}$; $IL_{e,0}/IL_{a,0} = 6\,\text{dB}$; $IL_{a,S,0}$ changes from $-35.98\,\text{dB}$ to $-30\,\text{dB}$, so that R_0 changes consequentially. For the upper trace, $N = 10^4$; for the middle trace, $N = 10^5$; for the lower trace, $N = 10^6$. For the numerically simulated traces, $T = 10^4$.

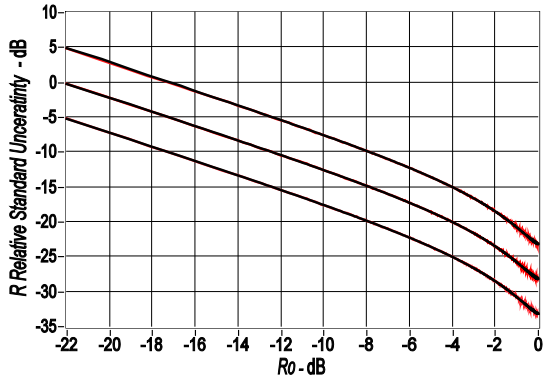

Figure 5. Numerical and analytical simulations of the relative standard uncertainty of R. The black traces are analytically simulated, whereas the red traces are numerically simulated. $IL_{e,0} = -30\,\text{dB}$; $IL_{e,0}/IL_{a,0} = 6\,\text{dB}$; $IL_{a,S,0}$ ranges from $-35.98\,\text{dB}$ to $-30\,\text{dB}$, so that R_0 changes consequentially. For the upper trace, $N = 10^4$; for the middle trace $N = 10^5$; for the lower trace, $N = 10^6$. For the numerically simulated traces, $T = 10^4$.

measurements as well. Clearly, for real measurements, it is difficult and time-consuming to achieve $T \gg 1$; therefore, the results corresponding to the numerical simulations can only be achieved approximately. However, the relevant uncertainty can be calculated. In the simulations where $T = 10000$, such an uncertainty is not appreciable. Actually, the simulations validated the achieved model.

Figures 6(a), 6(b), and 6(c) show the numerical and analytical simulations of R as a function of $IL_{a,S,0}$. The conditions of the traces in these figures correspond to the conditions of the traces in Fig. 5, except T, which is equal to 1, as shown in the relevant caption.

It is important to note that with the increase of the independent sample number, most of the measurement dynamic range is achieved for $IL_{a,S,0} < -35\,\text{dB}$, which corresponds to $R < -6\,\text{dB}$, i.e.,

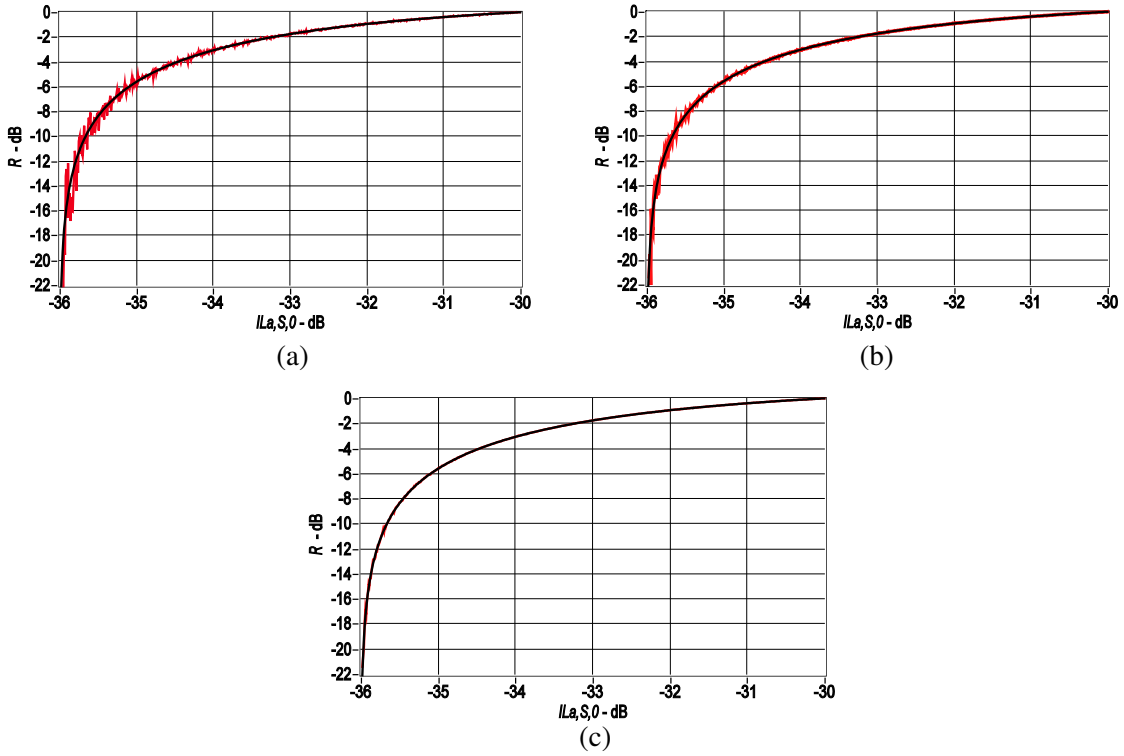

Figure 6. Numerical and analytical simulations of R. The black traces are analytically simulated, whereas the red traces are numerically simulated. $IL_{e,0} = -30\,\mathrm{dB}$; $IL_{e,0} - IL_{a,0} = 6\,\mathrm{dB}$; $IL_{a,S,0}$ ranges from -30 to $-35.98\,\mathrm{dB}$, so that R changes accordingly. N is 10^4, 10^5, and 10^6 in cases (a), (b), and (c), respectively. For the numerically simulated traces, $T = 1$.

for $R < -6\,\mathrm{dB}$, the measurement is more sensitive but less accurate. This is related to the fact that the uncertainty increases with the decrease of reflectivity coefficient R, as shown in Fig. 5.

One realizes that the increase of the measurement dynamic range for the reflectivity in an RC requires a high N value. We stress that if the measurements are taken for a sufficient number of configurations, which depends on N, then the relevant uncertainty is neutralized and can be neglected [22], as mentioned above. Therefore, in order to neglect the uncertainty due to the configuration, N samples have to be taken for different configurations [22]. It is convenient to make it in an automated way, so that the mode stirring, position stirring (or source stirring), and frequency stirring are combined in the same chamber [14, 22], and it avoids time-consuming measurement procedures.

4. MEASUREMENTS

The measurements were conducted in the RC at the Università Parthenope. The RC used for the measurements is a cubic chamber of $8\,\mathrm{m}^3$ volume, where the input electromagnetic field is randomized by means of three metallic stirrers rotating in continuous mode. Random mechanical stirring due to the vibrations of the chamber walls under the effect of the motors of the stirrers adds to the regular mechanical stirring, so that a very large number of independent samples can be acquired. It must be noted that the statistical independence of the acquired samples was verified by the autocorrelation function (not shown in the paper). The measurement set up includes two double-ridge waveguide horn antennas, model ETS-Lindgren 3115, and a two-ports Vector Network Analyzer (VNA), model Agilent 8363B PNA. An inside view of the chamber is shown in Fig. 7. The fixture used for the experiments is formed by a microwave plane absorber, model Emmerson & Cumming Eccosorb AN-W-79, which is placed in an aluminium case, so that only the top of the absorber can be exposed to the electromagnetic radiation. We specify that the fixture with the sample is accurately arranged by closing the edges of

the sample with adhesive aluminium tape. Note that the average residual reflectivity due to the real absorber used for the fixture [15] does not affect the results shown here, as the measurements, as well as the results, are guaranteed by the measured NL. However, when it is necessary, a systematic error can be properly removed.

We specify that the available measurements at the moment are made for one configuration only; therefore, the uncertainty due to the configuration of the measurement system is not neutralized. For this reason, we will compare the measurement results with the expected ones by using the extended uncertainty. However, except for this aspect, the model is tested in a simple and efficacious way. We devised samples under test for which the expected values are easy and accurately achieved, and we made a series of measurements from which R and the NL are achieved. The samples under test are obtained by covering a given percentage of the absorber surface by an aluminum sheet. The percentages of the covering are: 100% (expected R is 0 dB), 50% (expected R is -3 dB), 25% (expected R is -6 dB), and 10% (expected R is -10 dB). As an example, the absorber covered to a percentage of the 50% is shown in Fig. 8.

Figure 9 shows $IL_{e,0}$ and $IL_{a,0}$. Fig. 10 shows the ratio $IL_{e,0}/IL_{a,0}$. Actually, the ratio in dB between the two ILs can be read in Fig. 9 as well; however, it is directly evident in Fig. 10. The frequency range is 1–10 GHz, and the max frequency was chosen to limit the variation range in the ratio $IL_{e,0}/IL_{a,0}$, so that the NL and dynamic range are practically uniform in all the frequency range. It allows us to easily test the measurement model.

Specifically, the order of the measurements was IL_e, $IL_{a,1}$, $IL_{a,S,100}$, $IL_{a,S,50}$, $IL_{a,S,25}$, $IL_{a,S,10}$, $IL_{a,2}$, where $IL_{a,1}$ and $IL_{a,2}$ are two independent measurements with loaded chamber to achieve the NL according to the above-mentioned procedure. In particular, in our case, the load is the fixture with no sample under test. Clearly, the number after the subscript S denotes the percentage of covered surface.

Figure 7. Inside view of the RC used for experiments.

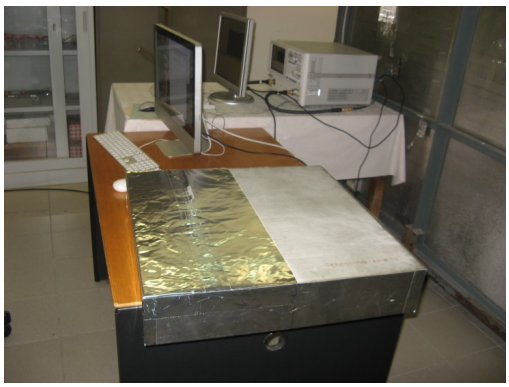

Figure 8. Absorber covered to a percentage of the 50%.

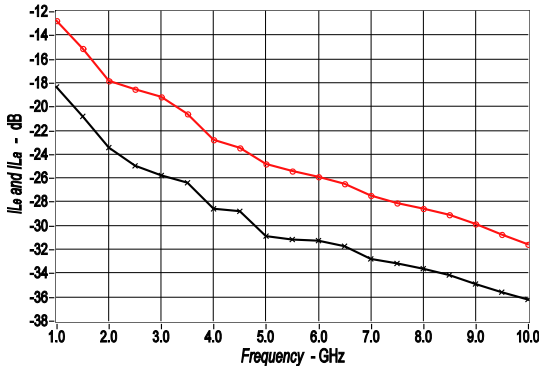

Figure 9. IL_e and IL_a of the RC used for experiments.

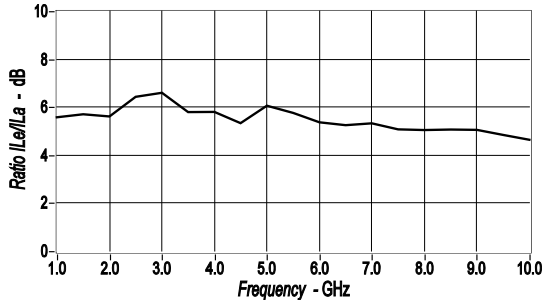

Figure 10. Ratio in dB between IL_e and IL_a of the RC used for experiments.

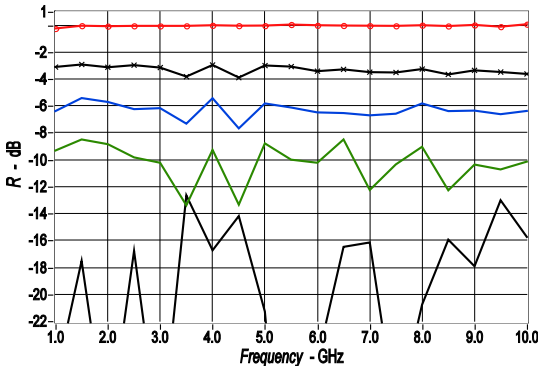

Figure 11. Measured R in dB. Except for the NL, which is represented by the bottom trace, from top to bottom, the expected values of R are 0, -3, -6, and -10 dB. These expected values correspond to percentages of covering of the absorbing surface of 100%, 50%, 25%, and 10%, respectively. The measurements include the error due to the configuration of the system.

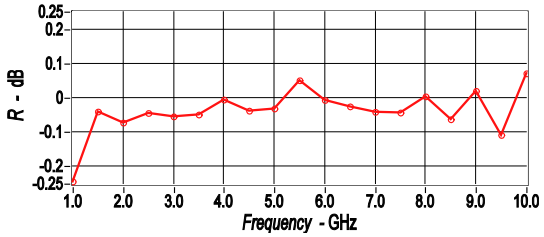

Figure 12. R in dB. Details of the R measurement corresponding to a percentages of covering of the absorbing surface of the 100%. The measurements include the error due to the configuration of the system.

The measurement setup is automated with LabVIEW, so that 10000 independent samples were automatically acquired (for each frequency) in as many frequency sweeps from 1 GHz to 10 GHz, with a step of 0.5 GHz. Therefore, N is 10^4 and $T = 1$; 21 frequency points were acquired for each sweep. Clearly, the sweep total number is equal to N. A random time uniformly distributed from 0 and 4 s was set between a sweep and the consecutive, in order to further guarantee the independence of the sample acquired at the same frequency. Note that the measurement setup is not automated with respect to the error due to the configuration of the system, i.e., the measurements were taken for one configuration only, as mentioned above. Actually, the hardware to automate the measurement setup with respect to the error due to the configuration was not available at the moment of the measurements.

Figure 11 shows the experimental results achieved by the measurements. The expected values of R are 0, -3, -6 and -10 dB from top to bottom. Fig. 12 shows the details of the trace regarding the expected value of 0 dB.

Note that the max value of the bottom trace is -12.6 dB, which corresponds to the frequency of 3.5 GHz. Therefore, the maximum NL is -12.6 dB. Note that the experimental results are in any case congruous with the results achieved by simulations in the previous section, even though the uncertainty due to the configuration was not neutralized. By considering the extended uncertainty with a coverage factor $k = 3$ [31], we have intervals having a level of confidence of 99.73 percent; they are equal to $8.2 \div -12.9$ dB for an expected value of -10 dB, $5.3 \div -6.9$ dB for an expected value of -6 dB, $-3 \div -2.7$ dB for an expected value of -3 dB and $-0.062 \div 0.063$ dB for an expected value of 0 dB. Therefore, all the measured values fall practically in the range of the extended uncertainty. We note that the measured values are slightly less than those expected, but by considering the extended uncertainty with a coverage factor $k = 3$, the ranges of the expected intervals practically include the measured ones. In Fig. 12, the first measured value of -0.23 dB corresponding to the expected value of 0 dB can be due to a slight departure from the requested field condition for IL_e and $IL_{a,S,100}$ measurements. Instead, regarding the traces slightly lower than those expected, the cause can be due to the location of the fixture with respect to the antennas and/or to the behavior non-uniform absorption of the absorber.

We point out that the uncertainty of the measured values of R can be reduced by taking the measurements for a number of sufficient configurations and by averaging them, so that the uncertainty and the NL depend only on N [22]. It is convenient to realize it by an automatized system, so that a proper combined stirring is achieved in the same chamber. For example, a solution is to achieve a combination of the mode stirring, position stirring (or source stirring), and frequency stirring. It optimizes the acquisition time as well.

5. CONCLUSION

The performance of the reflectivity measurement in an RC in terms of uncertainty and relevant NL has been shown. A good agreement between the analytical and numerical simulations is achieved, and measurements further confirm the validity of the results. The model for reflectivity measurement has been tested in a simple and efficacious way, by covering a given percentage of the absorber surface of the fixture by an aluminum sheet, so that the expected values are easily and accurately achieved. Since the uncertainty depending on the configuration of the measurement setup is not neutralized in the paper, the comparison between experimental and expected results is made by using the extended uncertainty, and a good agreement is observed between the experimental and expected results. However, in light of the fact that the ACS measurements can be averaged with respect to the configuration of the measurement setup, so that the relevant uncertainty depends only on the number of independent sample, the uncertainty and relevant measurement dynamic range of the reflectivity in an RC depend only on the number of independent measurements acquired. In order to neutralize the error due to the configuration, an automatized measurement system should be realized, so that a proper combined stirring is achieved. It optimizes the time of acquisition of the samples as well. Such a hardware to automate the measurement setup with respect to the error due to the configuration was not available at the moment of the measurements.

ACKNOWLEDGMENT

The authors thank Mr. Giuseppe Grassini of the Electrical and Electronic Measurements Lab (at Engineering Department, University of Napoli Parthenope) for helping in conducting the experiments that have been used in this paper.

APPENDIX A.

With reference to Eq. (2), the reflectivity coefficient R is given by the ratio between the RVs L and M. These last ones have an approximately normal distribution, as mentioned above (in the Section 2). In order to find the PDF of R, we show the correlation coefficients of L and M, given by Eq. (4), and the corresponding variation coefficients $cv_L = \sigma_L/\mu_L$ and $cv_M = \sigma_M/\mu_M$, respectively; they are shown in Figs. A1 and A2, respectively. Fig. A3 shows some details of the Fig. A2. We specify that cv_L and cv_M are obtained by the regarding equations in Section 2. We note that the correlation coefficient ranges

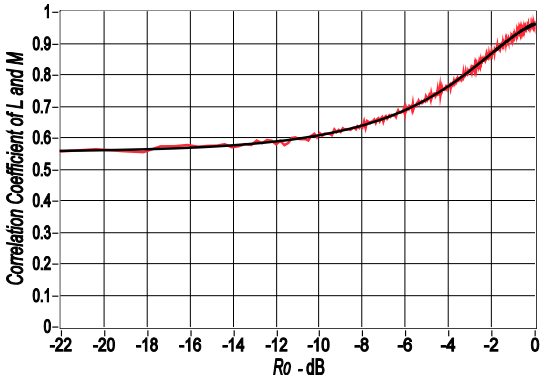

Figure A1. Analytically and numerically simulated correlation coefficient of the RVs L and M. $N = 10^4$; For the numerically simulated trace, $T = 10^4$. The black trace is analytically simulated, whereas the red trace is numerically simulated.

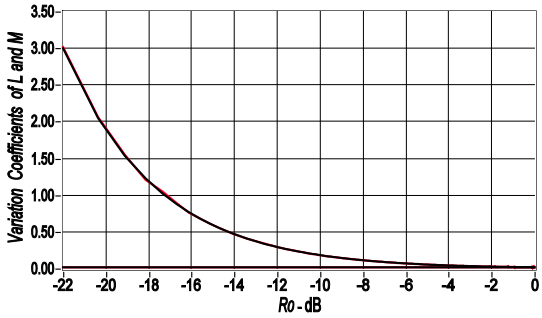

Figure A2. Analytically and numerically simulated variation coefficients of the RVs L and M. The traces higher regard L, whereas the lower traces regard the RV M. $N = 10^4$; For the numerically simulated trace, $T = 10^4$. The black traces are analytically simulated, whereas the red traces are numerically simulated.

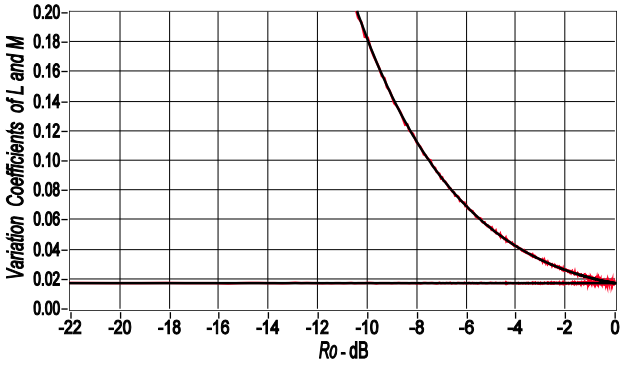

Figure A3. Details on the analytically and numerically simulated variation coefficients of the RVs L and M. The traces higher regard L, whereas the lower traces regard the RV M. $N = 10^4$; For the numerically simulated trace, $T = 10^4$. The black traces are analytically simulated, whereas the red traces are numerically simulated.

from 0.55 to 0.96. The variation coefficient of M is practically constant and equal to 0.017, whereas that of L ranges from a minimum of 0.017 to 3.07.

Note that if $R_0 \leq -8\,\text{dB}$, then R is approximately normal [33, 34]. It was verified on the numerically simulated data by the Chi-Square Goodness-of-Fit test by using LabVIEW again. We find that the normal approximation is achieved at the five percent significance level when N is much greater than one. If $N > 1000$, the approximation is accepted to the significance level of 0.05. One realizes that the worst conditions for the normal approximation of R occur when R is close to 1 (0 dB). In fact, the variation coefficient of L is minimum, and the correlation coefficient of L and M is maximum. However, we made various tests in the worst conditions for the normal approximation and other tests in better conditions in terms of correlation coefficient and variation coefficients of L and M. We find that the normal approximation is achieved at the five percent significance level when N is much greater than one. If $N > 1000$, the approximation is accepted to the significance level of 0.05, even if $\rho(X, Y)$ is at the greatest value. We specify that all the Chi-Square Goodness-of-Fit tests were done with a ratio between IL_e and IL_a greater or equal to 3 dB.

REFERENCES

1. IEC 61000-4-21, "Testing and measurement techniques — Reverberation chamber test methods," *Electromagnetic Compatibility (EMC)*, Part 4–21, International Electrotechnical Commission, Geneva, Switzerland, 2011.
2. Corona, P., M. Migliaccio, G. Ferrara, "Reverberating chambers as sources of stochastic electromagnetic fields enclosure for measurements of radiated power in the microwave range," *IEEE Trans. Electromagn. Compat.*, Vol. 38, 348–356, May 1996.
3. Corona, P., G. Latmiral, E. Paolini, and L. Piccioli, "Use of reverberating enclosure for measurements of radiated power in the microwave range," *IEEE Trans. Electromagn. Compat.*, Vol. 18, 54–59, May 1976.
4. Holloway, C. L., D. A. Hill, J. Ladbury, G. Koepke, and R. Garzia, "Shielding effectiveness measurements of materials using nested reverberation chambers," *IEEE Trans. Electromagn. Compat.*, Vol. 45, 350–356, May 2003.
5. Gifuni, A. and M. Migliaccio, "Use of nested reverberating chambers to measure shielding effectiveness of nonreciprocal samples taking into account multiple interactions," *IEEE Trans. Electromagn. Compat.*, Vol. 50, 783–786, November 2008.
6. Holloway, C. L., D. A. Hill, M. Sandroni, J. Ladbury, J. Coder, G. Koepke, A. C. Marvin, and Y. He, "Use of reverberation chambers to determine the shielding effectiveness of physically small, electrically large enclosures and cavities," *IEEE Trans. Electromagn. Compat.*, Vol. 50, 770–782, November 2008.

7. Fang, C.-H., S. Zheng, H. Tan, D. Xie, and Q. Zhang, "Shielding effectiveness measurements on enclosures with various apertures by both mode-tuned reverberation chamber and GTEM cell methodologies," *Progress In Electromagnetics Research B*, Vol. 2, 103–114, 2008.
8. Mariani, P. V., F. Moglie, and A. P. Pastore, "Field penetration through a wire mesh screen excited by a reverberation chamber field: FDTD analysis and experiments," *IEEE Trans. Electromagn. Compat.*, Vol. 51, No. 4, 883–891, November 2009.
9. Gifuni, A., G. Ferrara, M. Migliaccio, and A. Sorrentino, "Estimate of the shielding effectiveness of an electrically large enclosure made with pierced metallic plate in a well-stirred reverberation chamber," *Progress In Electromagnetics Research C*, Vol. 44, 133–144, 2013.
10. Lampasi, D. A. and M. S. Sarto, "Shielding effectiveness of a thick multilayered panel in a reverberating chamber," *IEEE Trans. Electromagn. Compat.*, Vol. 53, No. 3, 579–588, August 2011.
11. Gifuni, A., "Relation between the shielding effectiveness of an electric large enclosure and the wall material under uniform and isotropic field conditions," *IEEE Trans. Electromagn. Compat.*, Vol. 55, 1354–1357, December 2013.
12. Van De Beek, S., R. Vogt-Ardatjew, H. Schipper, and F. Leferink, "Vibrating intrinsic reverberation chambers for shielding effectiveness measurements," *Proc. IEEE, Int. Symp. EMC*, 1–6, Rome, IT, September 17–21, 2012.
13. Migliaccio, M., G. Ferrara, A. Gifuni, A. Sorrentino, F. Colangelo, C. Ferone, R. Cioffi, and F. Messina, "Shielding effectiveness tests of low-cost civil engineering materials in a reverberating chamber," *Progress In Electromagnetics Research B*, Vol. 54, 227–243, 2013.
14. Carlberg, U., P.-S. Kildal, A. Wolfang, O. Sotoudeh, and C. Orlenius, "Calculated and measured absorption cross sections of lossy objects in reverberation chamber," *IEEE Trans. Electromagn. Compat.*, Vol. 46, 146–154, May 2004.
15. Gifuni, A., "On the measurement of the absorption cross section and material reflectivity in a reverberation chamber," *IEEE Trans. Electromagn. Compat.*, Vol. 51, 1047–1050, November 2009.
16. Gradoni, G., D. Micheli, F. Moglie, and V. Mariani Primiani, "Absorbing cross section in reverberation chamber: Experimental and numerical results," *Progress In Electromagnetics Research B*, Vol. 45, 187–202, 2012.
17. Lalléchère, S., S. Girard, D. Roux, P. Bonnet, F. Paladian, and A. Vian, "Mode stirred reverberation chamber (msrc): A large and efficient tool to lead high frequency bioelectromagnetic *in vitro* experimentation," *Progress In Electromagnetics Research B*, Vol. 26, 257–290, 2010.
18. Melia, G. C. R., M. P. Robinson, I. D. Flintoft, A. C. Marvin, and J. F. Dawson, "Broadband measurement of absorption cross section of the human body in a reverberation chamber," *IEEE Trans. Electromagn. Compat.*, Vol. 55, 1043–1050, December 2013.
19. Senić, D., C. L. Holloway, J. M. Ladbury, G. H. Koepke, and A. Šarolić, "Absorption characteristics and SAR of a lossy sphere inside a reverberation chamber," *Proc. IEEE 2014 Int. Symp., EMC*, Gothenburg, Sweden, Sept. 1–4, 2014.
20. Holloway, C. L., H. A. Haider, R. J. Pirkl, W. F. Yong, D. A. Hill, and J. Ladbury, "Reverberation chamber techniques for determining the radiation and total efficiency of antennas," *IEEE Trans. Electromagn. Compat.*, Vol. 60, 1758–1770, April 2012.
21. Kildal, P.-S. and K. Rosengren, "Correlation and capacity of MIMO systems and mutual coupling, radiation efficiency, and diversity gain of their antennas: Simulations and measurements in a reverberation chamber," *IEEE Communication Magazine*, Vol. 42, 112, December 2004.
22. Gifuni, A., G. Ferrara, A. Sorrentino, and M. Migliaccio, "Analysis of the measurement uncertainty of the absorption cross section in a reverberation chamber," *IEEE Trans. Electromagn. Compat.*, Vol. PP, No. 99, 1–4, 2015, http://ieeexplore.ieee.org/stamp/stamp.jsp?tp=&arnumber=7167691.
23. Holloway, C. L., A. H. David, J. M. Ladbury, P. F. Wilson, G. Koepke, and J. Coder, "On the use of reverberation chambers to simulate a rician radio environment for the testing of wireless devices," *IEEE Trans. Electromagn. Compat.*, Vol. 54, 3167–3177, November 2006.
24. Ferrara, G., M. Migliaccio, and A. Sorrentino, "Characterization of GSM non-line-of-sight propagation channels generated in a reverberating chamber by using bit error rates," *IEEE Trans.*

Electromagn. Compat., Vol. 44, 467–473, August 2007.

25. Gender, E. G., C. L. Holloway, K. A. Remely, J. M. Ladbury, G. Koepke, and H. Garbe, "Simulating the multipath channel with a reverberation chamber: Application to bit error rate measurements," *IEEE Trans. Electromagn. Compat.*, Vol. 52, 766–777, November 2010.
26. Pomianek, A. J., K. Staniec, and Z. Joskiewicz, "Practical remarks on measurement and simulation methods to emulate the wireless channel in the reverberation chamber," *Progress In Electromagnetics Research*, Vol. 105, 49–69, 2010.
27. Gifuni, A., A. Sorrentino, G. Ferrara, M. Migliaccio, A. Fanti, and G. Mazzarella, "Measurements on the reflectivity of materials in a reverberating chamber," *Proc. Loughborough Antennas and Propagation Conf.*, 1–4, Loughborough, 2011.
28. Gifuni, A., "Metodologia di Misura dell'efficacia dello schermaggio elettromagnetico," *Università degli Studi di Napoli "Parthenope"*, Dipartimento per le Tecnologie, Napoli, 2005.
29. Aroian, L. A., "The probability function of the product of two normally distributed variables," *The Annals of Mathematical Statistics*, Vol. 18, 265–271, 1947.
30. Blumenfeld, D., *Operations Research Calculations Handbook*, CRC Press, New York, B. R. London, New York Washington, D.C., 2001.
31. Taylor, B. N. and C. E. Kuyatt, "Guidelines for evaluating and expressing the uncertainty of NIST measurement results," NIST Tech. Note 1297, September 1994.
32. Holloway, C. L., D. A. Hill, J. M. Ladbury, and G. Koepke, "Requirements for an effective reverberation chamber: Unloaded or loaded," *IEEE Trans. Electromagn. Compat.*, Vol. 48, No. 1, 187–193, February 2006.
33. Hayya, J., D. Armstrong, and N. Gressis, "A note on the ratio of two normally distributed variables," *Management Science*, Theory Series, Vol. 21, No. 11, 1338–1341, July 1975.
34. Hinkley, D. V., "On the ratio of two correlated normal random variables," *Biometrika*, Vol. 56, No. 3, 635–639, December 1960.